Targeting of the Osteoclastogenic RANKL–RANK Axis Prevents Osteoporotic Bone Loss and Soft Tissue Calcification in Coxsackievirus B3–Infected Mice

Kyunghee Lee, Hyunsoo Kim, Ho Sun Park, Keuk-Jun Kim, Hoogeun Song, Hong-In Shin, Han-Sung Kim, Donghyun Seo, Hyun Kook, Jeong-Hyeon Ko and Daewon Jeong

J Immunol 2013; 190:1623-1630; Prepublished online 9 January 2013;
doi: 10.4049/jimmunol.1201479
http://www.jimmunol.org/content/190/4/1623

The Journal of Immunology is published twice each month by
The American Association of Immunologists, Inc.,
9650 Rockville Pike, Bethesda, MD 20814-3994.

Print ISSN: 0022-1767 Online ISSN: 1550-6606.

Targeting of the Osteoclastogenic RANKL–RANK Axis Prevents Osteoporotic Bone Loss and Soft Tissue Calcification in Coxsackievirus B3–Infected Mice

Kyunghee Lee,[*,†,1] Hyunsoo Kim,[*,†,1,2] Ho Sun Park,[*] Keuk-Jun Kim,[‡] Hoogeun Song,[§] Hong-In Shin,[¶] Han-Sung Kim,[‖,#] Donghyun Seo,[‖,#] Hyun Kook,[,††] Jeong-Hyeon Ko,[**,††] and Daewon Jeong[*,†]**

Bone mineralization is a normal physiological process, whereas ectopic calcification of soft tissues is a pathological process that leads to irreversible tissue damage. We have established a coxsackievirus B3 (CVB3)–infected mouse model that manifests both osteoporosis and ectopic calcification specifically in heart, pancreas, and lung. The CVB3-infected mice showed increased serum concentrations of both cytokines including IL-1β, TNF-α, and the receptor activator of NF-κB ligand (RANKL) that stimulate osteoclast formation and of the osteoclast-derived protein tartrate-resistant acid phosphatase 5b. They exhibited more osteoclasts in bone, with no change in the number of osteoblasts, and a decrease in bone formation and the serum concentration of osteoblast-produced osteocalcin. These results indicate that CVB3-induced osteoporosis is likely due to upregulation of osteoclast formation and function, in addition to decreased osteoblast activity. In addition, the serum in the CVB3-infected mice contained a high inorganic phosphate content, which causes ectopic calcification. RANKL treatment induced an increase in the in vitro cardiac fibroblast calcification by inorganic phosphate via the upregulation of osteogenic BMP2, SPARC, Runx2, Fra-1, and NF-κB signaling. We finally observed that i.p. administration of RANK-Fc, a recombinant antagonist of RANKL, prevented bone loss as well as ectopic calcification in CVB3-infected mice. Thus, our results indicate that RANKL may contribute to both abnormal calcium deposition in soft tissues and calcium depletion in bone. In addition, our animal model should provide a tool for the development of new therapeutic agents for calcium disturbance in soft and hard tissues. ***The Journal of Immunology*****, 2013, 190: 1623–1630.**

Calcium is an essential element that plays a key role in the mineralization and maintenance of the skeleton as well as in such fundamental physiological processes as growth and development in vertebrates. Calcium homeostasis is precisely regulated through the coordination of intestinal absorption, renal reabsorption, and bone turnover (1). Bone contains ∼99% of total calcium in the human body and is a site for regulation of systemic calcium homeostasis (2, 3). The regulation of calcium homeostasis by bone is achieved by the coordinated action of bone-degrading osteoclasts and bone-forming osteoblasts. Osteoclasts are responsible for the resorption or degradation of mineralized extracellular matrix, which results in the release of calcium into the extracellular space and the circulation (4). Conversely, osteoblasts are responsible for the deposition of inorganic minerals including calcium into the extracellular matrix, resulting in the formation of hydroxyapatite as a major component of bone (2). In vertebrates, biomineralization has both physiological and pathological aspects. Physiological mineralization is essential for proper development and function of hard tissues, such as bone, teeth, and growth plate cartilage, but it does not occur in soft tissues. Pathological ectopic mineralization, in contrast, occurs in soft tissues, including blood vessels, kidney, articular cartilage, and cardiovascular tissue. This process is associated with promineralization factors, such as inflammation, high phosphate and calcium levels, and apoptotic cell death resulting from phosphate overload or inflammatory reactions, which eventually leads to serious clinical outcomes in

*Department of Microbiology, Yeungnam University College of Medicine, Daegu 705-717, Korea; †Aging-Associated Vascular Disease Research Center, Yeungnam University College of Medicine, Daegu 705-717, Korea; ‡Department of Clinical Pathology, Taekyeung College, Gyeungsan 712-719, Korea; §Department of Biological Sciences, National Creative Research Initiatives Center, Graduate School of Nanoscience and Technology, Korea Advanced Institute of Science and Technology, Daejeon 305-701, Korea; ¶Department of Oral Pathology, Institute for Hard Tissue and Bio-Tooth Regeneration, School of Dentristry, Kyungpook National University, Daegu 700-412, Korea; ‖Department of Biomedical Engineering, Institute of Medical Engineering, Yonsei University, Wonju 220-710, Korea; #Yonsei-Fraunhofer Medical Device Laboratory, Yonsei University, Wonju 220-710, Korea; **Department of Pharmacology, Chonnam National University Medical School, Gwangju 501-746, Korea; and ††Medical Research Center for Gene Regulation, Chonnam National University Medical School, Gwangju 501-746, Korea

[1]K.L. and H. Kim contributed equally to this study.

[2]Current address: Department of Pathology and Laboratory Medicine, University of Pennsylvania School of Medicine, Philadelphia, PA.

Received for publication May 29, 2012. Accepted for publication December 10, 2012.

This work was supported by grants (2011-0006178 and 2010-0012161 to D.J.) from the National Research Foundation of Korea by the Korean Government.

Address correspondence and reprint requests to Prof. Daewon Jeong, Department of Microbiology, Yeungnam University College of Medicine, 317-1 Daemyung-Dong, Nam-Gu, Daegu 705-717, Korea. E-mail address: dwjeong@ynu.ac.kr

The online version of this article contains supplemental material.

Abbreviations used in this article: BFR, bone-formation rate; BMD, bone mineral density; BV, bone volume; CAR, coxsackievirus and adenovirus receptor; μCT, micro–computed tomography; CVB3, coxsackievirus B3; DAF, decay-accelerating factor; MAR, mineral-apposition rate; OPG, osteoprotegerin; Pi, inorganic phosphate; RANK, receptor activator of NF-κB; RANKL, receptor activator of NF-κB ligand; TRACP5b, tartrate-resistant acid phosphatase 5b; TRAP, tartrate-resistant acid phosphatase.

www.jimmunol.org/cgi/doi/10.4049/jimmunol.1201479

humans (5). Calcification of articular cartilage, for example, is responsible for joint stiffness, whereas cardiovascular calcification gives rise to morbidity and mortality (6).

Coxsackieviruses are nonenveloped human pathogenic picornaviruses that belong to the enterovirus group and possess an ssRNA genome (7). Coxsackievirus B3 (CVB3) has previously been detected in multiple organs, including heart, pancreas, lung, small intestine, liver, brain, kidney, and spleen of infected mice (8). Such infection in humans has also been found to result in various inflammatory conditions, including myocarditis, pancreatitis, respiratory disease, gastroenteritis, hepatitis, meningitis, and encephalitis (9–11). Moreover, case reports have described individuals infected with CVB3 who manifest symptoms of calcification in the heart or liver, resulting in premature death, and with the tissue surrounding calcified lesions being found to be infiltrated with lymphocytes, macrophages, and neutrophils (12, 13). In acute viral myocarditis, CVB3 infection results in the migration and subsequent infiltration of NK cells into the heart, followed by a second wave of infiltration by Th cells and CTLs (14). The infiltrated immune cells produce proinflammatory cytokines, such as IL-1β and TNF-α, which results in an increase in the plasma levels of these factors and plays a key role in the histopathologic and immunologic responses associated with CVB3-induced myocarditis (15, 16). Although cumulative sporadic evidence has been suggestive of a link among virus infection, inflammation, and ectopic calcification, there has been no direct evidence of causal relations.

In humans, bone loss has been associated with a high prevalence of pathological ectopic calcification in soft tissues, as evidenced by clinical studies showing a correlation between decreased bone mass and increased soft tissue calcification (17–19). In addition, a close link between vascular calcification and bone destruction has been demonstrated using drugs, such as bisphosphonates. The anti-osteoporotic bisphosphonates were shown to inhibit arterial and cardiac calcification, resulting in a reduction in cardiovascular risk (20). Statins, which are effective in reducing vascular calcification in cardiovascular disease (21), have also been found to increase bone mass, showing an anabolic effect on bone in mice and osteoporotic patients (22).

The common regulators responsible for the connection between bone decalcification and soft tissue calcification are still unknown. To provide insight into such coordinated regulation and develop corresponding therapeutic agents, we established a novel mouse model of CVB3 infection that manifests both soft-tissue calcification and bone destruction. With the use of this model, we have identified a potential therapeutic target for both conditions.

Materials and Methods

Virus and mice

CVB3 (Nancy strain) was propagated in HeLa cells grown in DMEM (HyClone) supplemented with 10% FBS and antibiotics. The virus was titrated using the plaque assay to determine PFU per milliliter and stored at −80˚C until used. Six- to 7-wk-old BALB/c mice were obtained from Central Lab Animal (Seoul, Korea) and were maintained at the animal facility of Yeungnam University College of Medicine. All animal procedures were approved by the Institutional Review Board of Yeungnam University College of Medicine and were in accordance with the Guide for the Care and Use of Laboratory Animals.

Study design

Male mice at 7 wk of age were injected i.p. with CVB3 (5×10^4 PFU) in PBS or with PBS alone (control). Some animals were also injected at the same time as, as well as 5 and 10 d after, virus injection with receptor activator of NF-κB (RANK)-Fc (5 mg/kg, i.p.), a soluble chimeric protein consisting of the extracellular domain of RANK and the C region (Fc) of human Ig G1, which specifically blocks the binding of receptor activator of NF-κB ligand (RANKL) to its cognate receptor, RANK (23). Mice were killed at 14 d or the indicated times after viral infection for the collection of serum, the tibia, and soft tissues (heart, pancreas, lung, spleen, kidney, brain, liver, aorta, skeletal muscle, skin, fat, and testis). The extent of viral infection in tissues was evaluated by determining PFU per gram tissue weight or by measuring the number of copies of the CVB3 RNA genome using real-time PCR analysis. For the quantitative analysis of CVB3 RNA genome, the following primers (forward and reverse, respectively) were used: CVB3, 5′-GTATTCCTCCGGCCCCTGAA-3′ and 5′-TCGCTTCCGCTGAAAGGTTG-3′; and hypoxanthine phosphoribosyltransferase, 5′-GTAATGATCAGTCAACGGGGGAC-3′ and 5′-CCAGCAAGCTTGCAACCTTAACCA-3′. The amounts of coxsackievirus and adenovirus receptor (CAR) mRNA and CVB3 RNA genome were determined by the comparative Δ threshold cycle method using hypoxanthine phosphoribosyltransferase mRNA as the invariant control.

Histological analysis and calcium quantification

Paraffin-embedded sections of soft tissue (thickness of 4 μm) were depleted of paraffin and subjected to H&E staining for routine histological analysis or to von Kossa staining for visualization of calcium deposition. Images were acquired with an Aperio ScanScope Model T3 and analyzed with ImageScope software (Aperio Technologies). For quantification of calcium in heart, pancreas, and lung, the tissues were weighed, frozen immediately in liquid nitrogen, and pulverized with a mortar and pestle. The tissue fragments were suspended in 0.6 M HCl and rocked vigorously at 4˚C for 48 h, after which the suspension was centrifuged at $10{,}000 \times g$ for 10 min at 4˚C. The calcium content of the resulting supernatant was determined colorimetrically with the use of a QuantiChrome Calcium Assay Kit (BioAssay Systems) and normalized by tissue weight. For histological analysis of bone, the tibia was dissected free from the surrounding tissue and decalcified with 10% EDTA for 2 wk. After the tibia was sectioned at a thickness of 5 μm using a microtome, specimens were stained with H&E or for tartrate-resistant acid phosphatase (TRAP) with the use of a leukocyte acid phosphatase staining kit (Sigma-Aldrich), which was used for detection of osteoblasts and osteoclasts, respectively. The numbers of plump cytoplasmic cuboidal osteoblasts and multinucleated osteoclasts present on the surface of trabecular bone were counted by light microscopy.

Osteoporotic indices and bone histomorphometric analysis

Trabecular morphometry for the proximal tibia was performed by high-resolution micro–computed tomography (μCT) (model 1076 μCT; Skyscan). Bone loss indices, including bone mineral density (BMD), bone volume (BV), BV/total volume, trabecular thickness, trabecular number, and trabecular separation, were assessed from the μCT data. In addition, serum levels of tartrate-resistant acid phosphatase 5b (TRACP5b) were determined using a Mouse TRAP Assay (Immunodiagnostic Systems) as a direct measure of early commitment to the osteoclast lineage and a sign of osteoporosis. For dynamic histomorphometry analysis of bone, mice were injected i.p. with calcein (15 mg/kg body weight; Sigma-Aldrich) at the same time of CVB3 infection and 3 d before they were sacrificed at 9 d postinfection. The diaphyseal cortical bone of the tibia was then sectioned, and the calcein double-labeled bone surface was photographed to measure mineral-apposition rate (MAR) and bone-formation rate (BFR).

In vitro biomineralization assay

The cardiac ventricular fibroblasts were isolated from neonatal Sprague-Dawley rats by enzymatic dissociation, as described previously (24). To assess in vitro calcification, cardiac fibroblast cells (2×10^4 cells/well in 48-well plates) were cultured in DMEM containing 10% FBS and 3 mM inorganic phosphate (Pi; pH 7.4) in the absence or presence of 100 ng/ml RANKL. Mineralized nodule formation and calcium deposition were visualized by von Kossa staining and alizarin red S staining. In addition, the calcium content in cell was determined using a QuantiChrome Calcium Assay Kit (BioAssay Systems) and represented as micrograms per milligrams protein, as previously described (25).

Measurement of cytokine, calcium, and phosphate in serum

The concentration of osteoprotegerin (OPG) and RANKL in serum was measured with the use of a Quantikine ELISA Kit (R&D Systems). Serum levels of TNF-α and IL-1β were also determined with specific ELISA kits (Abfrontier, Seoul, Korea). The content of calcium and phosphate in serum was determined using a QuantiChrome Assay Kit (BioAssay Systems).

Quantitative real-time PCR and immunoblot analysis

Total RNA was isolated from cells with the use of the TRIzol reagent (Invitrogen). The RNA (2 μg) was subjected to real-time PCR analysis using SYBR Premix Ex Taq (Takara Bio). Quantitative real-time PCR was

performed according to the standard protocols of the Applied Biosystems 7500 Sequence Detection System and software (Applied Biosystems). Relative mRNA expression levels were determined by the comparative Δ threshold cycle method using *Gapdh* mRNA as the invariant control. Specific primers for osteogenic marker genes were synthesized by Bionics (Seoul, Korea) and listed in Supplemental Table I. For immunoblot analysis, cells were suspended in lysis buffer containing 20 mM Tris-HCl (pH 7.5), 150 mM NaCl, 1% Nonidet P-40, 0.5% sodium deoxycholate, 1 mM EDTA, 0.1% SDS, and protease inhibitors (Complete tablets; Roche Molecular Biochemicals). The suspension was centrifuged at 10,000 × *g* for 10 min at 4°C, and the protein concentration of the resulting supernatant was quantified using a DC protein assay (Bio-Rad). The supernatant was fractionated by SDS-PAGE on a 10% gel, and the separated proteins were transferred to a nitrocellulose membrane for immunoblot analysis with Abs to alkaline phosphatase, Runx2, Fra-1 (Santa Cruz Biotechnology), phospho-IκBα (Cell Signaling Technology), or β-actin (Santa Cruz Biotechnology). Immune complexes were detected with HRP-conjugated secondary Abs and ECL reagents (Abfrontier).

Statistical analysis

Quantitative data are presented as means ± SD from at least three independent experiments or the indicated numbers of mice, and data with more than three groups were assessed by ANOVA using the SPSS 18.0 software package (SPSS). When significant differences were found, pairwise comparisons between each group were performed using the two-tailed Student *t* test. A p value of <0.05 was considered statistically significant.

Results

CVB3-infected mice exhibit ectopic calcification in heart, pancreas, and lung

We first examined the pathological signs exhibited by male BALB/c mice after i.p. injection of CVB3. Microscopic examination with von Kossa staining of tissue sections from CVB3-infected mice revealed ectopic calcification in soft tissues. This calcification was also confirmed by quantifying tissue calcium content. As shown in Fig. 1, calcium levels in heart and pancreas were increased at 3 d after CVB3 infection, but pathological signs of calcium deposits were not observed in these tissues. On 7 d postinfection, calcification was detected in the heart and pancreas, and those tissues contained a high level of calcium when compared with control tissues. Ectopic calcification in heart and pancreas remained apparent for 14 d postinfection (Fig. 1A, 1B), at which time deposition of calcium in the lung was also observed (Fig. 1C). In histological analysis, calcium deposition was observed in cardiac muscle, necrotic acinar cells of the pancreas, and interstitial cells of the lung. However, other tissues, including spleen, kidney, brain, liver, aorta, skeletal muscle, skin, fat, and testis, did not show ectopic calcification in CVB3-infected mice (data not shown).

The CAR and decay-accelerating factor (DAF) play key roles in CVB3 infection as an internalization receptor and a coreceptor, respectively (26, 27). We next analyzed the relationship between ectopic calcification and CAR and DAF expression. The mRNA and protein levels of CAR in the tissues were in the following order: heart < lung < pancreas (Supplemental Fig. 1A, 1B). In contrast, the extent of viral infection in the tissues was in the following order: lung < pancreas < heart (Supplemental Fig. 1C, 1D). Consistent with previous findings (28), the extents of CAR expression and virus infection did not appear to correlate in the heart and pancreas. The tissue distribution of DAF protein was similar to that of CAR protein, with the exception that DAF was also moderately abundant in skeletal muscle (Supplemental Fig. 1B). As shown in Fig. 1, the extent of ectopic calcification in the tissue was in the following order: lung < heart < pancreas at 7 d postinfection and of lung < heart ≈ pancreas at 14 d. Together, these results suggested that the extents of CAR expression and viral infection are not related to the extent of ectopic calcification in heart and lung, although there is a tendency toward such a relation in pancreas.

CVB3 infection induces a severe osteoporotic phenotype due to increased osteoclast formation and function along with decreased osteoblast function

We next investigated the effect of CVB3 infection on bone remodeling. Trabecular bone microstructure analysis of long bones and lumbar vertebrae with high-resolution μCT revealed that CVB3-infected mice started to show bone defects 7 d after virus infection, even though this difference was not significant, which subsequently manifested an osteoporotic phenotype characterized by significant decreases in BMD, BV/total volume, and trabecular number as well as an increase in trabecular separation 14 d postinfection (Fig. 2A, Supplemental Fig. 1E). However, there was no change in BMD of cortical bone (Supplemental Fig. 1F, 1G). Both MAR and BFR were reduced in CVB3-infected mice compared

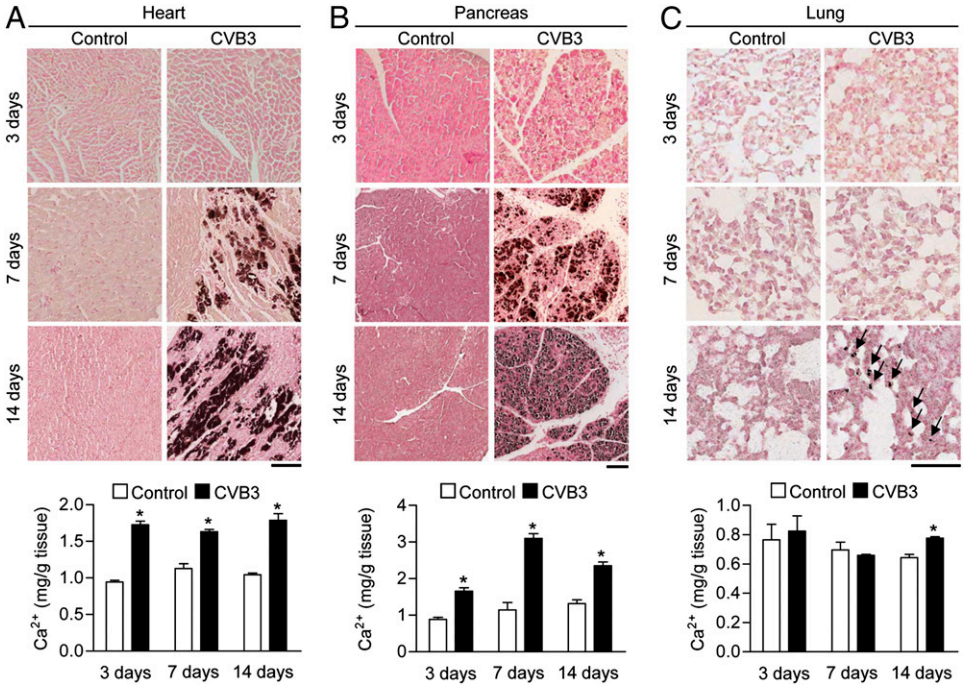

FIGURE 1. CVB3 infection induces ectopic calcification in heart, pancreas, and lung. Tissues [heart (**A**), pancreas (**B**), and lung (**C**)] from male mice at 3, 7, and 14 d after i.p. injection of CVB3 or from corresponding control animals were subjected to von Kossa staining of calcium deposits as well as quantification of calcium content. Arrows indicate calcium deposits in lung tissue. Quantitative data are expressed as milligrams of calcium per gram of tissue and are means ± SD (control mice, $n = 5$; CVB3-infected mice, $n = 6$). Scale bars, 100 μm. $^*p < 0.01$ versus the corresponding control value.

with control mice (Fig. 2B). Analysis of osteoblasts and osteoclasts on the trabecular bone surface by H&E and TRAP staining, respectively, revealed that the number of TRAP(+) osteoclasts markedly increased in CVB3-infected mice, whereas the number of osteoblasts was not affected by virus infection (Fig. 2C). Consistent with these findings, the serum level of TRACP5b, an early indicator of osteoclast formation and osteoporotic progression (29), as well as in vitro differentiation of osteoclast progenitors obtained from bone marrow both increased in CVB3-infected mice when compared with control mice (Fig. 2D). In contrast, the serum osteocalcin level, a marker of osteoblast functional activity, was markedly reduced by CVB3 infection (Fig. 2E) without any accompanying change in the number of osteoblasts on the trabecular bone surface (Fig. 2C). These results suggest that the bone loss associated with CVB3 infection was due, at least part, to increased bone resorption, resulting from increased osteoclast differentiation and function, and decreased osteoblast function.

We next examined the possibility that the immune response to CVB3, in particular an increased production of inflammatory cytokines that can stimulate osteoclast formation, was responsible for the osteoporotic phenotype of CVB3-infected mice. We found that the serum levels of RANKL, TNF-α, and IL-1β were significantly increased 7 and 14 d after CVB3 infection (Fig. 2F, Supplemental Fig. 2A). Consistent with this finding, CVB3 infection increased the T cell population that can produce RANKL as well as augmented the RANKL level in calcified tissues (Supplemental Fig. 2B, 2C). The level of OPG, which antagonizes RANKL function (30), was also elevated similar to that of RANKL, showing that the RANKL/OPG ratio was not altered by viral infection (Fig. 2F). Simultaneous increases in both RANKL and OPG levels could be the result of an enhanced immune response induced by CVB3 infection. This was confirmed by an increase in the myeloid lineage population that can differentiate into osteoclasts as well as higher recruitment of lymphocytes and macrophages to the heart and pancreas of CVB3-infected mice (Supplemental Fig. 2D, 2E), which is consistent with previous reports (12, 13). Based on these results, we propose that an increase in inflammatory cytokines and osteoclast progenitors in the virus-infected mice contributes to the stimulation of osteoclast differentiation and function, eventually leading to a reduction in bone mass.

RANKL stimulates cardiac fibroblast calcification induced by Pi

To further assess the causative factors of the observed soft tissue calcification, we analyzed serum levels of OPG, RANKL, calcium, and phosphate (Pi). As shown in Fig. 3A, the serum level of RANKL gradually increased after CVB3 infection. This was accompanied by an increase in the level of OPG. CVB3 infection induced elevated serum level of Pi at 14 d after CVB3 infection, but resulted in no change in calcium levels. A recent study demonstrated that Pi and RANKL were linked to vascular calcification (31, 32); therefore, we next examined the role of Pi and RANKL in the in vitro soft-tissue calcification. When cardiac primary cells (cardiac fibroblasts and myocytes) and cardiomyoblastic H9C2 cells were treated with Pi, a calcified phenomenon

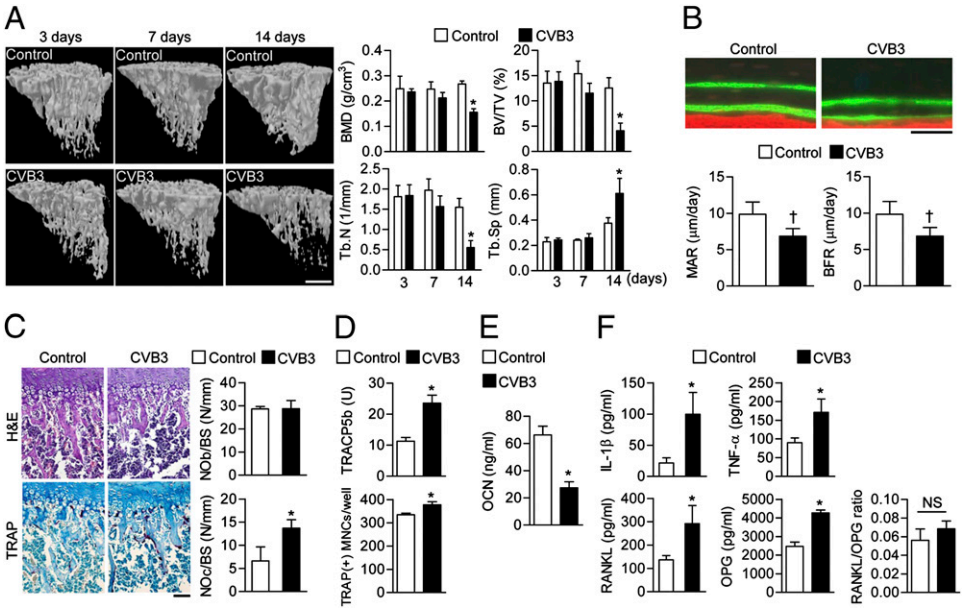

FIGURE 2. CVB3 infection results in the development of a severe osteoporotic phenotype. Bone parameters and the number of osteoblasts and osteoclasts were analyzed at various time points after CVB3 infection. (**A**) μCT analysis of the tibia of control and CVB3-infected mice. Representative images are shown in the *left panel*. Scale bar, 0.5 mm. Quantitative data for trabecular structural parameters are also presented as means ± SD (control mice, $n = 10$; CVB3-infected mice, $n = 22$). (**B**) MAR and BFR in the tibia were analyzed by the calcein double-labeling method. Scale bar, 100 μm. Data are means ± SD (control mice, $n = 8$; CVB3-infected mice, $n = 6$). (**C**) Fourteen days after CVB3 infection, osteoblasts and osteoclasts on the surface of trabecular bone from control and CVB3-infected mice were visualized by H&E and TRAP staining, respectively (*left panel*). Scale bar, 100 μm. The numbers of osteoblasts (NOb/BS) and osteoclasts per millimeter of trabecular bone surface (NOc/BS) (*right panel*) are also presented as means ± SD (control mice, $n = 10$; CVB3-infected mice, $n = 10$). (**D**) Osteoclast function and formation. To assess osteoclast activity, the serum concentration of TRACP5b was measured at 14 d after CVB3 infection. Data are means ± SD (control mice, $n = 10$; CVB3-infected mice, $n = 10$). To verify the extent of osteoclast formation, bone marrow–derived osteoclast progenitors prepared at 7 d after CVB infection were differentiated into osteoclasts in the presence of M-CSF (30 ng/ml) and RANKL (100 ng/ml) for 4 d. After TRAP staining, TRAP-positive multinucleated osteoclasts [TRAP(+) MNCs] containing >10 nuclei were counted under a light microscope. Data are the means ± SD ($n = 3$). *$p < 0.01$. (**E**) Serum concentration of osteocalcin (OCN), a marker of osteoblast activity, at 14 d after CVB3 infection. Data are the means ± SD (control mice, $n = 3$; CVB3-infected mice, $n = 8$). *$p < 0.01$. (**F**) Serum concentrations of IL-1β, TNF-α, RANKL, OPG, and RANKL/OPG ratio at 14 d after CVB3 infection. Data are means ± SD (control mice, $n = 10$; CVB3-infected mice, $n = 10$). *$p < 0.01$ versus the corresponding control value, †$p < 0.05$.

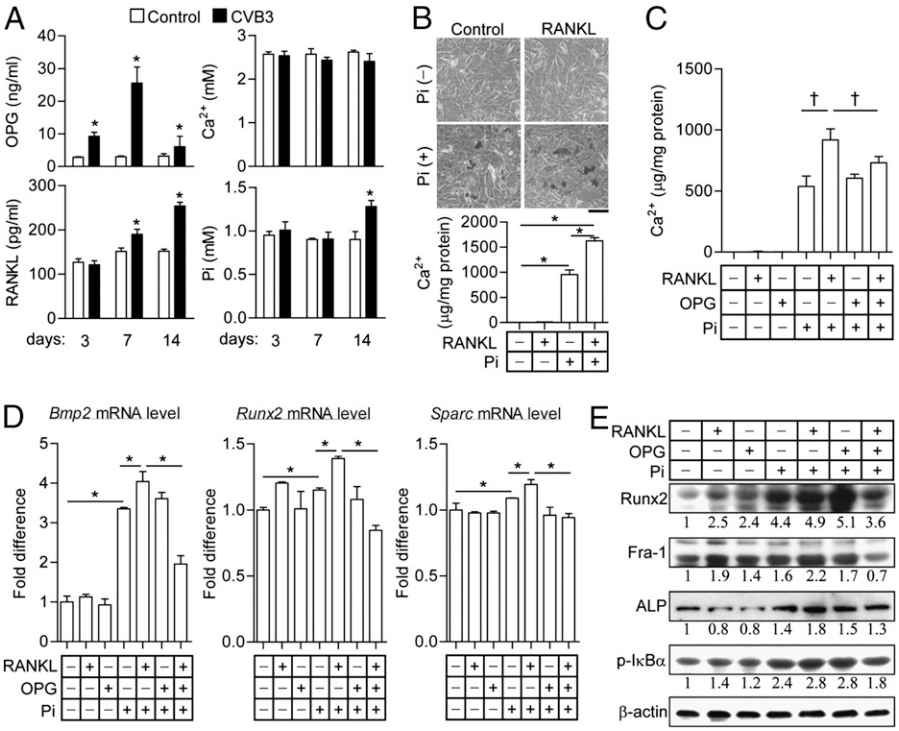

FIGURE 3. RANKL promotes Pi-induced cardiac fibroblast calcification. (**A**) Serum concentrations of OPG, RANKL, calcium, and Pi 3, 7, and 14 d after CVB3 infection. Data are means ± SD (control mice, $n = 3$; CVB3-infected mice, $n = 5$). *$p < 0.01$ versus the corresponding control value. (**B**) The synergic effect of RANKL on Pi-induced cardiac fibroblast calcification. Primary cardiac fibroblast cells were treated with 3 mM Pi in the absence or presence of 100 ng/ml RANKL for 3 d. Calcium content in cells was measured, and calcium deposits were visualized by von Kossa staining. A representative image is presented in the *top panel*. Scale bar, 100 μm. Quantitative data are means ± SD ($n = 3$). (**C** and **D**) Changes in calcium deposition and osteogenic marker gene levels upon treatment with RANKL and OPG. After cardiac fibroblasts were incubated with Pi in the absence or presence of RANKL (100 ng/ml) and OPG (100 ng/ml) for 3 d, the extent of calcium deposition in cells was measured (C). Data are the means ± SD ($n = 3$). Expression of osteogenic marker genes (*Bmp2* and *4*, *Runx2*, and *Sparc*) was analyzed by quantitative real-time PCR using *Gapdh* mRNA as a control (D). The mRNA level is represented as a fold difference relative to control. Data are the means ± SD ($n = 3$). (**E**) Immunoblot analysis for osteogenic marker proteins. Total cell lysates prepared from cardiac fibroblasts cultured with or without Pi, RANKL, and OPG for 3 d were subjected to immunoblot analysis with specific Abs to alkaline phosphatase (ALP), Runx2, Fra-1, p-IκBα, or β-actin (loading control). The band intensities are expressed as a fold difference relative to control. *$p < 0.01$, †$p < 0.05$.

was observed, which was characterized by nodule formation and calcium deposits (Supplemental Fig. 3A). Among the three cells tested, cardiac fibroblast cells were used in the subsequent experiment to conduct an in-depth analysis of soft-tissue calcification. Exogenous treatment with RANKL to cardiac fibroblast cells expressing RANK (Supplemental Fig. 3B), a cognate receptor of RANKL, induced synergic stimulation of cardiac fibroblast calcification caused by Pi, as visualized by von Kossa staining and verified by calcium quantification (Fig. 3B). The appearance of this calcified property was confirmed by increased calcium deposition and mRNA expression of osteogenic genes, including *Bmp2*, *Runx2*, and *Sparc*, at various concentrations of RANKL and at various time points following RANKL treatment (Supplemental Fig. 3C, 3D). RANKL-induced calcium deposition and osteogenic gene expression were both abolished by treatment with OPG, a decoy receptor for RANKL (Fig. 3C, 3D). Treatment with OPG induced inhibition of RANKL-mediated activation of osteogenic signals, including Runx2, Fra-1, and NF-κB (Fig. 3E), suggesting that the synergistic effect of RANKL on Pi-induced calcification was dependent on RANKL/RANK axis signaling. These findings suggest that ectopic soft-tissue calcification by CVB3 infection is likely caused by Pi alone and/or a combinatory action of Pi and RANKL.

RANK-Fc attenuates soft-tissue calcification and bone loss induced by CVB3 infection

Individuals with osteoporosis frequently experience vascular calcification, and ectopic arterial mineralization is often accompanied by decreased BMD (17, 33). RANKL, which is essential for osteoclast formation, has also been implicated in ectopic vascular calcification (32). We therefore next investigated whether the fusion construct RANK-Fc, which is able to block RANKL–RANK signaling and subsequent osteoclast formation (23), has the potential to prevent CVB3-induced ectopic calcification in our mouse model. As expected, we found that treatment with RANK-Fc prevented CVB3-induced bone defects, as revealed both by μCT analysis (Fig. 4A) and measurement of the serum levels of the osteoporotic marker TRACP5b (Fig. 4B), although it had no effects on the serum levels of RANKL and OPG (Fig. 4C). The increase in the number of osteoclasts on the surface of trabecular bone in CVB3-infected mice was also prevented by RANK-Fc treatment (Fig. 4D). Furthermore, we found that RANK-Fc administration prevented ectopic calcification in heart, pancreas, and lung induced by CVB3 infection (Fig. 5). Thus, these results suggest that RANKL–RANK signaling is a potential target for prevention of both bone loss and soft-tissue calcification induced by CVB3 infection.

Discussion

Many tissues, including heart, pancreas, lung, kidney, stomach, muscle, articular cartilage, and blood vessels, are susceptible to ectopic calcification (5, 34). In the current study, CVB3-infected mice manifested extensive calcification in the heart, pancreas, and lung. We observed pathological signs in BALB/c mice after i.p. injection of CVB3. At 3 d postinfection, the serum of infected

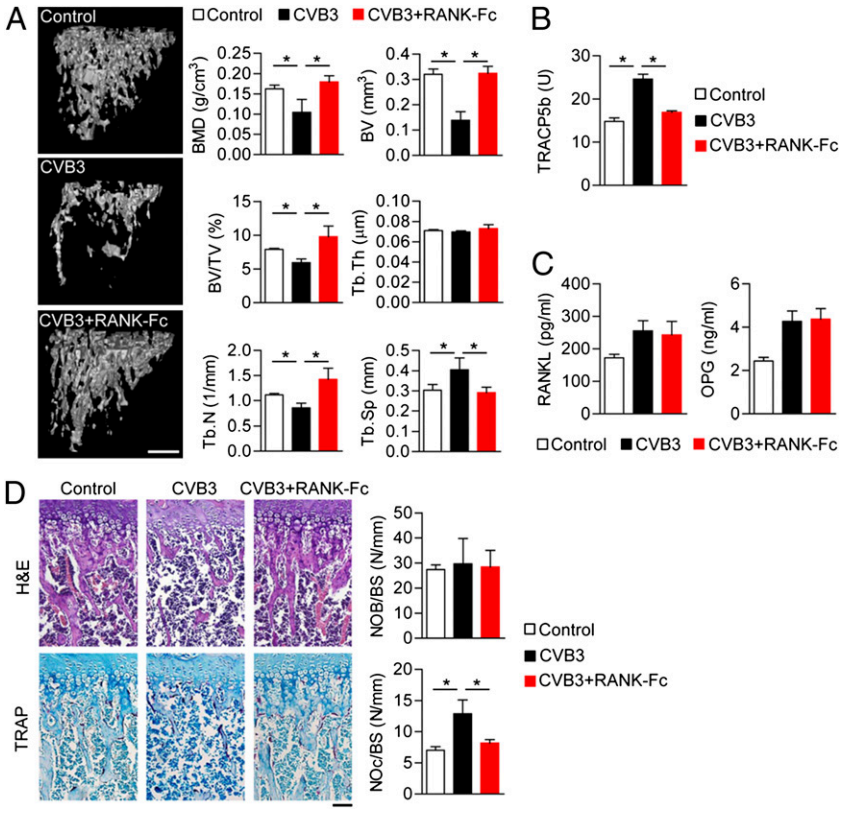

FIGURE 4. RANK-Fc prevents bone loss in CVB3-infected mice. (**A**) μCT analysis of the tibia of control mice or of CVB3-infected mice 14 d postinfection, with or without administration of RANK-Fc (5 mg/kg, i.p.) at 0, 5, and 10 d after virus injection. Scale bar, 0.5 mm. (**B** and **C**) Serum concentrations of TRACP5b, RANKL, and OPG in mice treated as in (A). (**D**) Osteoblasts and osteoclasts on the surface of trabecular bone of mice treated as in (A) were detected by H&E and TRAP staining, respectively, and counted. Scale bar, 100 μm. Quantitative data in all panels are means ± SD (n = 5/group). *$p < 0.01$. BV/TV, BV/total volume; NOb/BS, numbers of osteoblasts per millimeter of trabecular bone surface; NOc/BS, numbers of osteoclasts per millimeter of trabecular bone surface; Tb.N, trabecular number; Tb.Sp, trabecular spacing; Tb.Th, trabecular thickness.

mice contained neutralizing Abs that were able to block virus infection of HeLa cells in vitro (data not shown), indicating that the mice had developed an immune response to CVB3. Ectopic calcification was not observed in heart, pancreas, and lung. After 7 d, pathological symptoms of CVB3 infection were observed with calcium deposits in heart and pancreas. Histological analysis of tissue sections stained with H&E revealed that viral infection resulted in increased infiltration of lymphocytes and macrophages into the heart and pancreas when compared with control mice (Supplemental Fig. 2E). Consistently, CVB3 infection in mice induced an increase in the number of myeloid progenitors (Supplemental Fig. 2D) and in the serum levels of inflammatory cytokines, including IL-1β, TNF-α, and RANKL (Supplemental Fig. 2A). At 14 d postinfection, calcification in the heart, pancreas, and lung was observed in CVB3-infected mice and the serum levels of inflammatory cytokines, including IL-1β, TNF-α, and RANKL, were markedly increased (Fig. 2F). Our data were consistent with previous reports that vascular calcification was associated with inflammation, possibly as a result of the release of multiple cytokines by activated immune cells at the inflammatory site (35, 36). In addition to apparent soft-tissue calcification, we also observed a high level of Pi in the serum (Fig. 3A), which is

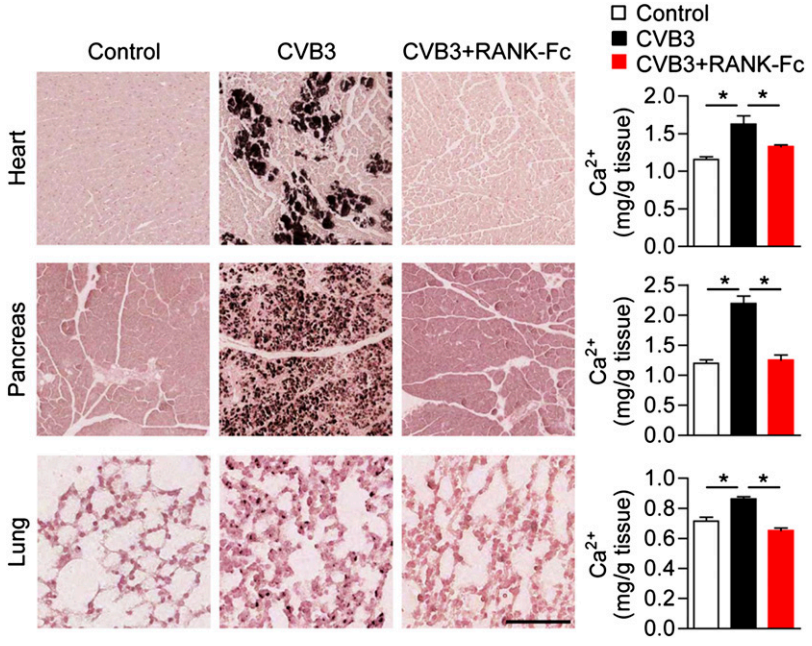

FIGURE 5. RANK-Fc prevents soft-tissue calcification induced by CVB3 infection. Tissue from control and CVB3-infected mice 14 d postinfection, with or without administration of RANK-Fc (5 mg/kg, i.p.), at 0, 5, and 10 d after virus injection was subjected to von Kossa staining of calcium deposits (*left panel*) as well as quantification of calcium content (*right panels*). Quantitative data are means ± SD (n = 5 mice/group). *$p < 0.01$. Scale bar, 100 μm.

one of major causative factors of vascular calcification (37). Furthermore, we demonstrated that RANKL stimulates Pi-induced cardiac fibroblast calcification in vitro via the activation of osteogenic signals, such as BMP2, SPARC, Runx2, Fra-1, and NF-κB (38–41). Taken together, our present data as well as previous findings suggest that inflammation or inflammatory cytokines may be involved in the entire process of soft-tissue calcification by CVB3 infection. However, we could not exclude the possibility that the high phosphate concentration in serum may play a role in soft-tissue calcification during the late stage of the experiment.

We found that CVB3 infection in mice led to a severe osteoporotic phenotype. After virus infection, CVB3-infected mice displayed an osteoporotic tendency 7 d postinfection and an apparent osteoporotic phenotype 14 d postinfection. One of the common host responses to CVB3 infection is an increase in the serum levels of cytokines (42). Furthermore, activated T cells capable of secreting multiple cytokines were previously shown to be closely associated with increased RANKL expression and consequent increased osteoclastic activity in bone (43). The main contributor to CVB3-induced bone loss in our mouse model was likely the increased serum concentrations of RANKL, TNF-α, and IL-1β, all of which stimulate osteoclastogenesis and bone resorption (44–46). We also found that CVB3-infected mice showed increased osteoclast numbers and activity, whereas osteoblast activity decreased with no change in cell numbers (Fig. 2C–E) and had a higher number of myeloid progenitors that can differentiate into osteoclasts (Supplemental Fig. 2D). In addition, the serum level of TRACP5b, a direct indicator of early commitment to the osteoclast lineage (29) and a sign of osteoporosis, was increased in CVB3-infected mice. We therefore conclude that CVB3-induced osteoporosis was due to increased osteoclast formation and bone-resorbing function, both of which are stimulated by inflammatory cytokines produced from immune cells of the virus-infected host, along with decreased osteoblast bone formation.

Several clinical case reports and genetically engineered animal models have suggested that osteoporosis is linked to vascular calcification, with the two conditions frequently occurring at the same time (17–19). Our present results show that CVB3-infected mice exhibited both ectopic calcification of soft tissues and bone loss, thus supporting a link between ectopic calcification and osteoporosis. Judging from the increased serum level of Pi at 14 d after virus infection, which coincided with the appearance of severe osteoporosis, it is possible that hyperphosphatemia caused by bone destruction may be associated with ectopic calcification. It has been reported that RANKL and TNF-α stimulate vascular calcification as well as osteoclastogenesis (36, 45, 47), and mice lacking OPG, which acts as a decoy receptor for RANKL and consequently inhibits osteoclast formation, exhibited osteoporosis and arterial calcification (48). Indeed, the RANKL–RANK–OPG system has been suggested to be a key regulator of bone metabolism (45) and a possible direct mediator of vascular calcification (32, 48). In general, this system is regulated by a counterbalance between RANKL and OPG (30). However, our present mouse model that displayed osteoporosis and ectopic calcification could not be applied to the general concept of RANKL/OPG system because CVB3-infected mice showed a concurrent increase in both RANKL and OPG, without any change in the RANKL/OPG ratio. On the basis of such previous findings and our present results, we suggest that RANKL and inflammatory cytokines, such as TNF-α and IL-1β, are common mediators of CVB3-induced ectopic calcification and osteoporosis, with RANKL possibly playing the predominant role. Indeed, we found that RANK-Fc, a recombinant protein that comprises the extracellular domain of RANK fused to the Fc region of human Ig G and inhibits osteoclast formation dependent on the RANKL–RANK axis (23), prevented both bone loss and soft-tissue calcification induced by CVB3 infection. Based on these results, despite the increased level of OPG, which plays a similar role as RANK-Fc in CVB3-infected mice, CVB3 infection was shown to induce osteoporosis and ectopic calcification, and exogenous administration of RANK-Fc blocked both pathological processes. Presumably, RANK-Fc may prevent osteoporosis through its efficient delivery to the bone environment compared with OPG and ectopic calcification due to the high RANK-Fc/OPG ratio in systemic circulation. Consistent with our results, denosumab, a human mAb to RANKL that directly blocks RANKL action, was recently shown to retard vascular calcification in knockin mice expressing humanized RANKL (49).

The present and previous observations suggest that agents capable of neutralizing RANKL action, including RANK-Fc, denosumab, and OPG, could be potential therapeutic agents for the prevention or attenuation of ectopic calcification in soft tissues. The new animal model described in the current study, which develops both ectopic calcification and osteoporosis, should prove useful for further characterization of the pathogenesis under these conditions as well as provide a tool for the development of new therapeutic agents for their treatment.

Acknowledgments

We thank J. Choi (Department of Pathology, Yeungnam University College of Medicine, Daegu, Korea) for helpful discussion on histological analysis and Y. Choi (University of Pennsylvania, Philadelphia, PA) for kindly providing RANK-Fc and RANKL.

Disclosures

The authors have no financial conflicts of interest.

References

1. Peacock, M. 2010. Calcium metabolism in health and disease. *Clin. J. Am. Soc. Nephrol.* 5(Suppl 1): S23–S30.
2. Zaidi, M. 2007. Skeletal remodeling in health and disease. *Nat. Med.* 13: 791–801.
3. Boskey, A. L., and R. Coleman. 2010. Aging and bone. *J. Dent. Res.* 89: 1333–1348.
4. Robinson, L. J., H. C. Blair, J. B. Barnett, M. Zaidi, and C. L. Huang. 2010. Regulation of bone turnover by calcium-regulated calcium channels. *Ann. N. Y. Acad. Sci.* 1192: 351–357.
5. Murshed, M., and M. D. McKee. 2010. Molecular determinants of extracellular matrix mineralization in bone and blood vessels. *Curr. Opin. Nephrol. Hypertens.* 19: 359–365.
6. Kirsch, T. 2006. Determinants of pathological mineralization. *Curr. Opin. Rheumatol.* 18: 174–180.
7. Esfandiarei, M., and B. M. McManus. 2008. Molecular biology and pathogenesis of viral myocarditis. *Annu. Rev. Pathol.* 3: 127–155.
8. Mena, I., C. M. Perry, S. Harkins, F. Rodriguez, J. Gebhard, and J. L. Whitton. 1999. The role of B lymphocytes in coxsackievirus B3 infection. *Am. J. Pathol.* 155: 1205–1215.
9. Chatterjee, N. K., D. W. Moore, S. S. Monroe, R. I. Glass, M. J. Cambridge, S. F. Kondracki, and D. L. Morse. 2004. Molecular epidemiology of outbreaks of viral gastroenteritis in New York State, 1998-1999. *Clin. Infect. Dis.* 38(Suppl 3): S303–S310.
10. Monto, A. S., A. M. Fendrick, and M. W. Sarnes. 2001. Respiratory illness caused by picornavirus infection: a review of clinical outcomes. *Clin. Ther.* 23: 1615–1627.
11. Muir, P., and A. M. van Loon. 1997. Enterovirus infections of the central nervous system. *Intervirology* 40: 153–166.
12. Oka, K., K. Oohira, Y. Yatabe, T. Tanaka, K. Kurano, R. Kosugi, M. Murata, H. Hakozaki, T. Nishikawa, and Y. Tsutsumi. 2005. Fulminant myocarditis demonstrating uncommon morphology—a report of two autopsy cases. *Virchows Arch.* 446: 259–264.
13. Konen, O., V. Rathaus, S. Bauer, T. Dolfin, and M. Shapiro. 2000. Progressive liver calcifications in neonatal coxsackievirus infection. *Pediatr. Radiol.* 30: 343–345.
14. Seko, Y., Y. Shinkai, A. Kawasaki, H. Yagita, K. Okumura, F. Takaku, and Y. Yazaki. 1991. Expression of perforin in infiltrating cells in murine hearts with acute myocarditis caused by coxsackievirus B3. *Circulation* 84: 788–795.
15. Lane, J. R., D. A. Neumann, A. Lafond-Walker, A. Herskowitz, and N. R. Rose. 1992. Interleukin 1 or tumor necrosis factor can promote Coxsackie B3-induced myocarditis in resistant B10.A mice. *J. Exp. Med.* 175: 1123–1129.

16. Fairweather, D., S. Frisancho-Kiss, S. Gatewood, D. Njoku, R. Steele, M. Barrett, and N. R. Rose. 2004. Mast cells and innate cytokines are associated with susceptibility to autoimmune heart disease following coxsackievirus B3 infection. *Autoimmunity* 37: 131–145.
17. Persy, V., and P. D'Haese. 2009. Vascular calcification and bone disease: the calcification paradox. *Trends Mol. Med.* 15: 405–416.
18. Hyder, J. A., M. A. Allison, M. H. Criqui, and C. M. Wright. 2007. Association between systemic calcified atherosclerosis and bone density. *Calcif. Tissue Int.* 80: 301–306.
19. Schulz, E., K. Arfai, X. Liu, J. Sayre, and V. Gilsanz. 2004. Aortic calcification and the risk of osteoporosis and fractures. *J. Clin. Endocrinol. Metab.* 89: 4246–4253.
20. Price, P. A., S. A. Faus, and M. K. Williamson. 2001. Bisphosphonates alendronate and ibandronate inhibit artery calcification at doses comparable to those that inhibit bone resorption. *Arterioscler. Thromb. Vasc. Biol.* 21: 817–824.
21. Callister, T. Q., P. Raggi, B. Cooil, N. J. Lippolis, and D. J. Russo. 1998. Effect of HMG-CoA reductase inhibitors on coronary artery disease as assessed by electron-beam computed tomography. *N. Engl. J. Med.* 339: 1972–1978.
22. Edwards, C. J., D. J. Hart, and T. D. Spector. 2000. Oral statins and increased bone-mineral density in postmenopausal women. *Lancet* 355: 2218–2219.
23. Sordillo, E. M., and R. N. Pearse. 2003. RANK-Fc: a therapeutic antagonist for RANK-L in myeloma. *Cancer* 97(Suppl): 802–812.
24. Kee, H. J., G. H. Eom, H. Joung, S. Shin, J. R. Kim, Y. K. Cho, N. Choe, B. W. Sim, D. Jo, M. H. Jeong, et al. 2008. Activation of histone deacetylase 2 by inducible heat shock protein 70 in cardiac hypertrophy. *Circ. Res.* 103: 1259–1269.
25. Kim, H., H. J. Kim, K. Lee, J. M. Kim, H. S. Kim, J. R. Kim, C. M. Ha, Y. K. Choi, S. J. Lee, J. Y. Kim, et al. 2012. α-Lipoic acid attenuates vascular calcification via reversal of mitochondrial function and restoration of Gas6/Axl/Akt survival pathway. *J. Cell. Mol. Med.* 16: 273–286.
26. Shafren, D. R., D. T. Williams, and R. D. Barry. 1997. A decay-accelerating factor-binding strain of coxsackievirus B3 requires the coxsackievirus-adenovirus receptor protein to mediate lytic infection of rhabdomyosarcoma cells. *J. Virol.* 71: 9844–9848.
27. Bergelson, J. M., J. A. Cunningham, G. Droguett, E. A. Kurt-Jones, A. Krithivas, J. S. Hong, M. S. Horwitz, R. L. Crowell, and R. W. Finberg. 1997. Isolation of a common receptor for Coxsackie B viruses and adenoviruses 2 and 5. *Science* 275: 1320–1323.
28. Shi, Y., C. Chen, U. Lisewski, U. Wrackmeyer, M. Radke, D. Westermann, M. Sauter, C. Tschöpe, W. Poller, K. Klingel, and M. Gotthardt. 2009. Cardiac deletion of the Coxsackievirus-adenovirus receptor abolishes Coxsackievirus B3 infection and prevents myocarditis in vivo. *J. Am. Coll. Cardiol.* 53: 1219–1226.
29. Halleen, J. M., S. L. Alatalo, H. Suominen, S. Cheng, A. J. Janckila, and H. K. Väänänen. 2000. Tartrate-resistant acid phosphatase 5b: a novel serum marker of bone resorption. *J. Bone Miner. Res.* 15: 1337–1345.
30. Lacey, D. L., E. Timms, H. L. Tan, M. J. Kelley, C. R. Dunstan, T. Burgess, R. Elliott, A. Colombero, G. Elliott, S. Scully, et al. 1998. Osteoprotegerin ligand is a cytokine that regulates osteoclast differentiation and activation. *Cell* 93: 165–176.
31. Reynolds, J. L., A. J. Joannides, J. N. Skepper, R. McNair, L. J. Schurgers, D. Proudfoot, W. Jahnen-Dechent, P. L. Weissberg, and C. M. Shanahan. 2004. Human vascular smooth muscle cells undergo vesicle-mediated calcification in response to changes in extracellular calcium and phosphate concentrations: a potential mechanism for accelerated vascular calcification in ESRD. *J. Am. Soc. Nephrol.* 15: 2857–2867.
32. Panizo, S., A. Cardus, M. Encinas, E. Parisi, P. Valcheva, S. López-Ongil, B. Coll, E. Fernandez, and J. M. Valdivielso. 2009. RANKL increases vascular smooth muscle cell calcification through a RANK-BMP4-dependent pathway. *Circ. Res.* 104: 1041–1048.
33. Hofbauer, L. C., C. C. Brueck, C. M. Shanahan, M. Schoppet, and H. Dobnig. 2007. Vascular calcification and osteoporosis—from clinical observation towards molecular understanding. *Osteoporos. Int.* 18: 251–259.
34. Chan, E. D., D. V. Morales, C. H. Welsh, M. T. McDermott, and M. I. Schwarz. 2002. Calcium deposition with or without bone formation in the lung. *Am. J. Respir. Crit. Care Med.* 165: 1654–1669.
35. Abedin, M., Y. Tintut, and L. L. Demer. 2004. Vascular calcification: mechanisms and clinical ramifications. *Arterioscler. Thromb. Vasc. Biol.* 24: 1161–1170.
36. Tintut, Y., J. Patel, F. Parhami, and L. L. Demer. 2000. Tumor necrosis factor-alpha promotes in vitro calcification of vascular cells via the cAMP pathway. *Circulation* 102: 2636–2642.
37. Giachelli, C. M. 2004. Vascular calcification mechanisms. *J. Am. Soc. Nephrol.* 15: 2959–2964.
38. Delany, A. M., I. Kalajzic, A. D. Bradshaw, E. H. Sage, and E. Canalis. 2003. Osteonectin-null mutation compromises osteoblast formation, maturation, and survival. *Endocrinology* 144: 2588–2596.
39. Tanaka, T., H. Sato, H. Doi, C. A. Yoshida, T. Shimizu, H. Matsui, M. Yamazaki, H. Akiyama, K. Kawai-Kowase, T. Iso, et al. 2008. Runx2 represses myocardin-mediated differentiation and facilitates osteogenic conversion of vascular smooth muscle cells. *Mol. Cell. Biol.* 28: 1147–1160.
40. Nakagawa, Y., K. Ikeda, Y. Akakabe, M. Koide, M. Uraoka, K. T. Yutaka, R. Kurimoto-Nakano, T. Takahashi, S. Matoba, H. Yamada, et al. 2010. Paracrine osteogenic signals via bone morphogenetic protein-2 accelerate the atherosclerotic intimal calcification in vivo. *Arterioscler. Thromb. Vasc. Biol.* 30: 1908–1915.
41. Jochum, W., J. P. David, C. Elliott, A. Wutz, H. Plenk, Jr., K. Matsuo, and E. F. Wagner. 2000. Increased bone formation and osteosclerosis in mice overexpressing the transcription factor Fra-1. *Nat. Med.* 6: 980–984.
42. Ilbäck, N. G., L. Wesslén, K. Pauksen, T. Stålhandske, G. Friman, and J. Fohlman. 1993. Effects of the antiviral WIN 54954 and the immune modulator LS 2616 on cachectin/TNF and gamma-interferon responses during viral heart disease. *Scand. J. Infect. Dis. Suppl.* 88: 117–123.
43. Kong, Y. Y., U. Feige, I. Sarosi, B. Bolon, A. Tafuri, S. Morony, C. Capparelli, J. Li, R. Elliott, S. McCabe, et al. 1999. Activated T cells regulate bone loss and joint destruction in adjuvant arthritis through osteoprotegerin ligand. *Nature* 402: 304–309.
44. Jimi, E., I. Nakamura, T. Ikebe, S. Akiyama, N. Takahashi, and T. Suda. 1998. Activation of NF-kappaB is involved in the survival of osteoclasts promoted by interleukin-1. *J. Biol. Chem.* 273: 8799–8805.
45. Boyle, W. J., W. S. Simonet, and D. L. Lacey. 2003. Osteoclast differentiation and activation. *Nature* 423: 337–342.
46. Lam, J., S. Takeshita, J. E. Barker, O. Kanagawa, F. P. Ross, and S. L. Teitelbaum. 2000. TNF-alpha induces osteoclastogenesis by direct stimulation of macrophages exposed to permissive levels of RANK ligand. *J. Clin. Invest.* 106: 1481–1488.
47. Kudo, O., Y. Fujikawa, I. Itonaga, A. Sabokbar, T. Torisu, and N. A. Athanasou. 2002. Proinflammatory cytokine (TNFalpha/IL-1alpha) induction of human osteoclast formation. *J. Pathol.* 198: 220–227.
48. Bucay, N., I. Sarosi, C. R. Dunstan, S. Morony, J. Tarpley, C. Capparelli, S. Scully, H. L. Tan, W. Xu, D. L. Lacey, et al. 1998. osteoprotegerin-deficient mice develop early onset osteoporosis and arterial calcification. *Genes Dev.* 12: 1260–1268.
49. Helas, S., C. Goettsch, M. Schoppet, U. Zeitz, U. Hempel, H. Morawietz, P. J. Kostenuik, R. G. Erben, and L. C. Hofbauer. 2009. Inhibition of receptor activator of NF-kappaB ligand by denosumab attenuates vascular calcium deposition in mice. *Am. J. Pathol.* 175: 473–478.